# Ignition and Transition to Flame Spread Over a Thermally Thin Cellulosic Sheet in a Microgravity Environment

K. NAKABE,* K. B. McGRATTAN, T. KASHIWAGI, H. R. BAUM, H. YAMASHITA,† and G. KUSHIDA†

*Building and Fire Research Laboratory, National Institute of Standards and Technology, Gaithersburg, MD 20899*

An axisymmetric, time-dependent model is developed describing auto-ignition and subsequent transition to flame spread over a thermally-thin cellulosic sheet heated by external radiation in a quiescent microgravity environment. Due to the unique combination of a microgravity environment and low Reynolds number associated with the slow, thermally induced flow, the resulting velocity is taken as a potential flow. A one-step global gas phase oxidation reaction and three global degradation reactions for the condensed phase are used in the model. A maximum external radiant flux of 5 W/cm$^2$ (Gaussian distribution) with 21%, 30%, and 50% oxygen concentrations is used in the calculations. The results indicate that autoignition is observed for 30% oxygen concentrations but the transition to the flame spread does not occur. For 50% oxygen the transition is achieved. A detailed discussion of the transition from ignition to flame spread is given as an aid to understanding this process. Also, a comparison is made between the axisymmetric configuration and a two-dimensional (line source) configuration.

## NOMENCLATURE

| | |
|---|---|
| $A$ | preexponential frequency factor |
| $c_p$ | specific heat |
| $c_s$ | specific heat of the solid fuel |
| $D$ | mass diffusivity |
| $E$ | activation energy |
| $G$ | Green's function |
| $h$ | enthalpy |
| $k$ | thermal conductivity |
| $k_x$ | reaction rate of solid phase reactions |
| $\dot{m}$ | mass flux |
| $\dot{q}_R$ | absorbed external radiation flux |
| $R$ | universal gas constant |
| $T$ | temperature |
| $t$ | time |
| $\vec{u}$ | solenoidal component of velocity |
| $\vec{v}$ | velocity vector |
| $r$ | radial coordinate |
| $z$ | axial coordinate normal to the paper surface |
| $Y$ | mass fraction |

### Greek Symbols

| | |
|---|---|
| $\gamma$ | reflectivity |
| $\delta$ | half thickness of thin solid sheet |
| $\epsilon$ | emissivity |
| $\Delta H$ | heat of reaction |
| $\nu$ | stoichiometric coefficient |
| $\rho$ | density |
| $\sigma$ | Stefan–Boltzmann constant |
| $\Phi$ | remainder potential function |
| $\phi$ | potential function |

### Subscripts

| | |
|---|---|
| $\infty$ | ambient condition |
| 0 | initial condition |
| $s$ | solid phase |
| $p$ | solid phase pyrolysis |
| ox | solid phase oxidative degradation |
| char | solid phase char oxidative degradation |
| $f$ | gaseous fuel |
| sf | solid fuel |
| $O_2$ | oxygen |

## INTRODUCTION

Ignition of solid fuels by external thermal radiation is a process that not only is of consider-

* Guest researcher from Osaka University, Osaka, Japan.
† Guest researchers from Nagoya University, Nagoya, Japan.



0010-2180/94/$7.00

able scientific interest but which also has fire safety applications. This process is complicated due to strong coupling between chemical reactions and transport processes not only in the gas phase but also in the condensed phase. Although the fundamental processes involved in radiative autoignition (without any external pilot) have been suggested [1–4], there have been no definitive experimental or modeling studies due to the flow motion generated by buoyancy near the heated sample surface. One must solve the time-dependent Navier–Stokes equations over an extended region to represent the highly unstable buoyant plume accurately. It is especially important to provide correct far field boundary conditions, particularly for velocities. A calculation was recently conducted for a piloted ignition of a liquid pool with specified velocity boundary conditions and without including gas-phase reactions [5]. In order to avoid the specification of the boundary conditions, previous detailed radiative ignition models were assumed to be one dimensional [6, 7] or were applied at the stagnation point [8, 9]. The mismatch between experimental and calculated geometries in normal gravity means that theories cannot be compared directly with experimental results except for specific configurations under which the plume is not formed.

In order to overcome the above difficulty, the authors are conducting a theoretical and experimental study for ignition and subsequent transition to flame spread in a microgravity environment for which buoyancy can be ignored. The objective of this study is to compare the theoretical results quantitatively to the experimental data and to obtain a more definitive understanding of the ignition and transition mechanism by taking advantage of the microgravity assumption. Furthermore, the model can be used for the examination of fire safety issues in a spacecraft. The fire safety strategy in a spacecraft is (1) to detect any fire as early as possible, (2) to keep any fire as small as possible, and (3) to extinguish any fire as quickly as possible [10, 11]. This suggests that a material that undergoes a momentary ignition might be tolerable but a material which permits a transition to flame spread would significantly increase the fire hazard in a spacecraft. Therefore, a model that has the capability to predict the transition from ignition to flame spread in a microgravity environment might be used for material screening for a spacecraft.

The first phase of the theoretical portion of this study [12] considered the two-phase heat and mass transfer problem associated with the thermal degradation of a thin cellulosic sample undergoing radiative heating. This paper extends that work by including a global exothermic gas phase oxidation reaction of the degradation products from the cellulosic material. This extension enables us to calculate ignition and the transition to flame spread. The theoretical model has been developed to be comparable to possible experiments in microgravity using NASA's two drop towers or the Space Shuttle. A thermally thin cellulosic sheet is considered as the sample fuel. Such a sample might ignite during test times available in the drop towers without requiring a pilot. The autoignition mode eliminates many parameters of a pilot such as its location, temperature, and size. In the autoignition mode the generation of high-temperature char at the sample surface by external radiation and by highly exothermic char oxidation acts as a self-induced pilot [1]. Although a slow flow along the sample surface, similar to a ventilation flow in a spacecraft, can have significant effects on flame spread velocity [13], a quiescent axisymmetric configuration is used first to develop the model. Currently, the extension of the model to a three-dimensional configuration with a slow flow along the sample surface is under way.

## THEORETICAL MODEL

The study of radiative ignition of solid fuels in a microgravity environment requires a description of time-dependent processes in both the gas and solid phase. The mathematical and computational complexity inherent in such a study suggests that any simplifications permitted by the microgravity environment and the small physical scale of the idealized experiment be built into the mathematical model. These simplifications principally affect the gas-phase processes. First, the absence of gravity removes the buoyancy-induced vorticity.

Second, the small scale of the experiment ($\sim$ 1 cm), together with the absence of any significant externally imposed velocity, implies a low Reynolds number flow. Classical analyses of low Reynolds number flows have demonstrated that using the Oseen approximation to the convective terms in the equations of motion "constitutes an *ad hoc* uniformization" [14] by a first approximation to the rigorous calculation of the flow past isolated bodies. The main point of these asymptotic expansions in Reynolds number is that diffusion dominates convection near the surface, so the fact that the Oseen flow does not satisfy the no-slip boundary condition is irrelevant at lowest order in the theory. When surface pyrolysis or evaporation is present, the thermally induced surface blowing velocity must be taken into account, even at low Reynolds numbers [12]. These effects can be accommodated by assuming the velocity field to be a potential flow. The uniform Oseen velocity used in classical analysis is indeed a trivial potential flow. The generalization to a flow past an arbitrarily shaped body with a prescribed surface blowing distribution can also be accommodated by a potential field, if vorticity generated in the interior of the flow can be ignored.

The conservation equations of mass, energy and species in the gas phase under low Mach number combustion and heat transfer conditions can be written

$$\frac{D\rho}{Dt} + \rho\nabla\cdot\vec{v} = 0, \tag{1}$$

$$\rho\frac{Dh}{Dt} - \nabla\cdot(k\nabla T) = \Delta H_f\dot{m}_f + \dot{q}_R, \tag{2}$$

$$\rho\frac{DY_{O_2}}{Dt} - \nabla\cdot(\rho D\nabla Y_{O_2}) = -\nu_{O_2}\dot{m}_f, \tag{3}$$

$$\rho\frac{DY_f}{Dt} - \nabla\cdot(\rho D\nabla Y_f) = -\dot{m}_f, \tag{4}$$

where $h = \int_0^T c_p(T)\,dT$. The gas-phase oxidation reaction is represented by a global one step reaction

$$[\text{Fuel Gas}] + \nu_{O_2}[\text{Oxygen}] \rightarrow [\text{Product}] \tag{5}$$

characterized by an Arrhenius rate term

$$\dot{m}_f = A\rho^2 Y_{O_2}Y_f \exp\left(-\frac{E}{RT}\right). \tag{6}$$

Diffusion flames with reaction rates of this form have been analyzed in detail [15].

The conservation equations above are supplemented by an equation of state, taken in a form appropriate for low Mach number flows

$$\rho h = \rho_\infty h_\infty. \tag{7}$$

Multiplying Eq. 1 by $h$ and adding it to Eq. 2 then yields

$$\rho_\infty h_\infty\nabla\cdot\vec{v} - \nabla\cdot(k\nabla T) = \Delta H_f\dot{m}_f + \dot{q}_R. \tag{8}$$

Eq. 8 is the fundamental equation for determining the velocity field $\vec{v}$, which can be decomposed into the sum of the gradient of a potential $\phi$ and a divergence-free solenoidal field

$$\vec{v} = \nabla\phi + \vec{u}. \tag{9}$$

Substitution of Eq. 9 into Eq. 8 yields

$$\nabla^2\phi = \frac{\Delta H_f\dot{m}_f + \dot{q}_R + \nabla\cdot(k\nabla T)}{\rho_\infty h_\infty}. \tag{10}$$

It is convenient to work with a remainder potential $\Phi$ whose Laplacian may be written

$$\nabla^2\Phi = \frac{\Delta H_f\dot{m}_f + \dot{q}_R}{\rho_\infty h_\infty}. \tag{11}$$

Equations 10 and 11 relate the potential field to the temperature distribution in the gas phase. Implied in this statement is the assumption that the solenoidal velocity field $\vec{u}$ is not of interest; otherwise there is no alternative to solving the Navier–Stokes equations. However, a large portion of both the combustion and heat transfer literature consists of a calculations in which the details of the velocity field are approximated, often crudely, in order to understand the thermophysical phenomenon of direct interest. In the present circumstances, the approximations have been justified in simple geometries by detailed analyses, and interest will be confined to temperature fields induced by radiative ignition and subsequent flame spread. The absorption of the external radiation by evolved degradation products in the gas [1, 9] is not included in the model because a tungsten lamp, which emits the majority of its energy in the near infrared, will be

used to reduce the absorption as much as possible in the planned experiment. Under these circumstances, the term $\dot{q}_R$ can be neglected.

The boundary conditions for the gas phase equations are provided by the solid fuel reactions. It is assumed that the cellulosic sheet is thermally thin and also of uniform composition through its depth. The pyrolysis of the cellulosic sheet is described by two global thermal degradation reactions and a char oxidation reaction. The detailed derivation of these reactions and their kinetic constants are described in Ref. 16. A brief description of the reaction model is given here for the convenience of readers.

(1) Endothermic global Pyrolysis reaction

$$\text{Cellulose} \rightarrow \nu_{\text{char},p}\text{Char} + \nu_{\text{sf},p}(\text{H}_x\text{C}_y + \text{CO}) + (1 - \nu_{\text{char},p} - \nu_{\text{sf},p}) \times (\text{H}_2\text{O} + \text{CO}_2). \quad (12)$$

(2) Exothermic global thermal Oxidative degradation reaction

$$\text{Cellulose} + \nu_{\text{O}_2,\text{ox}}\text{O}_2 \rightarrow \nu_{\text{char,ox}}\text{Char} + \nu_{\text{sf,ox}}(\text{H}_x\text{C}_y + \text{CO}) + (1 + \nu_{\text{O}_2,\text{ox}} - \nu_{\text{char,ox}} - \nu_{\text{sf,ox}}) \times (\text{H}_2\text{O} + \text{CO}_2). \quad (13)$$

(3) Exothermal global Char oxidation reaction

$$\text{Char} + \nu_{\text{O}_2,\text{char}}\text{O}_2 \rightarrow \nu_{\text{ash,char}}\text{Ash} + \nu_{\text{sf,char}}(\text{H}_x\text{C}_y + \text{CO}) + (1 + \nu_{\text{O}_2,\text{char}} - \nu_{\text{ash,char}} - \nu_{\text{sf,char}}) \times (\text{H}_2\text{O} + \text{CO}_2). \quad (14)$$

The combustible gases consist of hydrocarbons ($\text{H}_x\text{C}_y$) and CO and the noncombustible gases consist of $\text{CO}_2$ and $\text{H}_2\text{O}$. It is assumed that the combustible gases formed from each reaction above are the same. Although these reactions are grossly approximated compared with the actual, extremely complex degradation reactions, their accuracy is at least comparable to that of the global one-step gas-phase oxidation reaction for the combustible gases, which is used as the sole gas phase reaction in this study.

The rate of each reaction above is approximately expressed by the following Arrhenius-type equations:

$$k_p = A_p(\rho_s Y_{\text{sf}}/\rho_{s_0})^{n_p} \exp(-E_p/RT_s),$$

$$k_{\text{ox}} = A_{\text{ox}}(\rho Y_{\text{O}_2}/\rho_{0,\text{ox}})^{n_{\text{ox}}} \cdot (\rho_s Y_{\text{sf}}/\rho_{s_0})^{n_{f,\text{ox}}} \exp(-E_{\text{ox}}/RT_s),$$

$$k_{\text{char}} = A_{\text{char}}(\rho Y_{\text{O}_2}/\rho_{0,\text{char}})^{n_{\text{O}_2,\text{char}}} \cdot (\rho_s Y_{\text{char}}/\rho_{s_0})^{n_{\text{char}}} \exp(-E_{\text{char}}/RT_s).$$

Values for the above kinetic parameters together with the heats of reaction $\Delta H_i$ for a particular black cellulosic paper[1] are taken from Ref. 16. The terms $\rho_{0,\text{ox}}$ and $\rho_{0,\text{char}}$ are the reference gas densities for oxidative degradation reaction and char oxidation reaction, respectively. The density of air at 573 K for the former reaction and 700 K for the latter are chosen because these reactions occur near these temperatures [16].[2] The equations for the condensed phase are given as follows:

Conservation of solid mass

$$\frac{\partial \rho_s/\rho_{s_0}}{\partial t} = -(1 - \nu_{\text{char},p})k_p - (1 - \nu_{\text{char,ox}})k_{\text{ox}} - (1 - \nu_{\text{ash,char}})k_{\text{char}}. \quad (15)$$

[1] Initially, a more well-defined ashless paper was used as a test sample. However, the surface reflectivity of this sample with respect to the emission from a tungsten lamp is so high that no ignition was observed in preliminary radiative ignition experiments in normal gravity. Therefore, a black paper was used as a sample although it is not as pure as the filter paper.

[2] However, the peak reaction rate depends on the heating rate and it shifts towards higher temperatures at higher heating rates. Therefore, a slight error could occur in the calculation of reaction rate. The error is well within the accuracy of the three derived reaction rates determined in Ref. 16.

Conservation of initial cellulosic material

$$\frac{\partial(\rho_s Y_{sf}/\rho_{s_0})}{\partial t} = -k_p - k_{ox}. \quad (16)$$

Conservation of char

$$\frac{\partial(\rho_s Y_{char}/\rho_{s_0})}{\partial t} = \nu_{char,p}k_p + \nu_{char,ox}k_{ox} - k_{char}. \quad (17)$$

Conservation of energy

$$\delta\rho_s c_s \frac{\partial T_s}{\partial t} = (-\Delta H_p k_p - \Delta H_{ox}k_{ox} - \Delta H_{char}k_{char}) \times \rho_{s_0}\delta + (1-\gamma)\dot{q}_{ex} - \epsilon\sigma(T_s^4 - T_0^4) + k\frac{\partial T}{\partial z} + \dot{m}(h_s - h). \quad (18)$$

The term $\partial T/\partial z$ is the normal derivative of the gas phase temperature at the sample surface, $\delta$ the half-thickness, $\rho_{s_0}$ the initial density and $c_s$ the specific heat of the paper. The heat flux of the external radiation is given by $\dot{q}_{ex}$, the reflectivity by $\gamma$ and the emissivity by $\epsilon$.

The boundary conditions at the sample surface ($z = 0$) can be expressed in terms of these quantities through the boundary conditions

$$T = T_s, \quad (19)$$

$$\dot{m}_{sf} = \dot{m}Y_f - \rho D\frac{\partial Y_f}{\partial z}, \quad (20)$$

$$\dot{m}_{O_2} = \dot{m}Y_{O_2} - \rho D\frac{\partial Y_{O_2}}{\partial z}, \quad (21)$$

$$\frac{\partial\Phi}{\partial z} = \frac{1}{\rho_\infty h_\infty}\left(h\dot{m} - k\frac{\partial T}{\partial z}\right), \quad (22)$$

where the fuel, oxygen and total mass flux from the sample, $\dot{m}_{sf}$, $\dot{m}_{O_2}$, and $\dot{m}$, are written in terms of the solid-phase reaction rates

$$\dot{m}_{sf} = [\nu_{sf,p}k_p + \nu_{sf,ox}k_{ox} + \nu_{sf,char}k_{char}]\rho_{s_0}\delta, \quad (23)$$

$$\dot{m}_{O_2} = [-\nu_{O_2,ox}k_{ox} - \nu_{O_2,char}k_{char}]\rho_{s_0}\delta, \quad (24)$$

$$\dot{m} = [(1-\nu_{char,p})k_p + (1-\nu_{char,ox})k_{ox} + (1-\nu_{ash,char})k_{char}]\rho_{s_0}\delta. \quad (25)$$

Far from the surface, $\phi$, $Y_i$, and $T$ must decay to their ambient initial values. Translating this into boundary conditions suitable for numerical computation, however, requires some care. Numerical boundary conditions are applied at the edge of a finite computational domain. Since $Y_i$ and $T$ decay exponentially to their ambient values, setting these quantities equal to their ambient values is permissible until the first calculated non-ambient contours of these quantities approach the computational boundary. However, the potential field decays slowly away from the heated region, i.e., $\phi \sim 1/(r^2 + z^2)$. Thus, putting $\phi$ or its gradient equal to zero at the computational boundary would introduce unacceptable error into the calculation. These errors can be avoided by using an analytical solution to Eq. 11 valid for the semi-infinite domain ($z > 0$) subject to the boundary condition given by Eq. 22 at the sample surface ($z = 0$).

$$\Phi(r,z,t) = \int_0^\infty\int_0^\infty \nabla^2\Phi G(r,z;r',z')r'\,dr'\,dz' + \int_0^\infty \frac{\partial\Phi}{\partial z}G(r,z;r',0)r'\,dr', \quad (26)$$

where $\nabla^2\Phi$ is given by Eq. 11, and $\partial\Phi/\partial z$ is given by Eq. 22. The Green's function is given by

$$G(r,z;r',z') = \frac{1}{\pi}\left(\frac{K(k_+)}{\sqrt{(r+r')^2 + (z+z')^2}} + \frac{K(k_-)}{\sqrt{(r+r')^2 + (z-z')^2}}\right) \quad (27)$$

where

$$k_+^2 = \frac{4rr'}{(r+r')^2 + (z+z')^2},$$

$$k_-^2 = \frac{4rr'}{(r+r')^2 + (z-z')^2},$$

and $K(k_\pm)$ are complete elliptic integrals of the first kind. Although these formulas are too cumbersome to use everywhere in the domain of interest, the fact that the temperature and chemical species fields decrease exponentially means that they can be used to calculate efficiently rigorous boundary conditions at the edge of the computational domain.

## NUMERICAL METHOD

The solid phase reactions, Eqs. 15–18, are solved using an ordinary differential equation stiff solver. The equations for temperature and species (Eqs. 2–4) are solved using an operator-splitting technique. The algorithm is a variant of a class of operator splitting schemes analyzed by Wichman [17] for problems involving high Damköhler numbers. The time marching algorithm is divided into two stages. The first stage follows the spatially homogeneous reaction in each cell of the quantities $Y_{O_2}$, $Y_f$, and $T$, solving Eqs. 2–4 without the convective-diffusive terms. The second stage redistributes these quantities by way of the convective-diffusive transport using the Dufort–Frankel scheme with time steps of 0.0005 s. The calculation is performed using finite difference techniques on a staggered grid with all scalar quantities evaluated at cell centers and velocity components on cell faces. Large gradients normal to the sample surface dictate that the grid spacing in the normal direction near the surface be of the order of 0.25 mm. In order to achieve this, it is necessary to employ a nonuniform spacing in the normal coordinate. Grid spacing in the radial direction is on the order of 1 mm.

Finally, Eq. 11 is solved using an efficient Poisson solver. The boundary conditions for $\Phi$ are specified at the open boundary by evaluating Eq. 26 at each time step. The volume integral can be evaluated efficiently by summing over a coarse grid, but with the source points of Green's function evaluated at the centroid of the integrand for each subvolume. The errors introduced by this procedure are negligible compared with the discretization errors.

## RESULTS

A schematic diagram of the axisymmetric configuration is shown in Fig. 1. Numerical calculations were conducted for three different gas-phase oxygen concentrations ($Y_{O_2,\infty}$ = 0.21, 0.30, 0.50) to determine the effects of gas-phase oxygen concentration on ignition and the subsequent transition to flame spread. The external radiation beam is applied to the material surface at the origin of the coordinates. The heat flux distribution $\dot{q}_{ex}$ is initially assumed to be Gaussian with a peak of 5 W/cm$^2$ and half width of 1 cm.[3] The reflectivity is assumed to be 0 and the emissivity is assumed to be 1. The half-thickness of the cellulosic material used in the present study is 0.0038 cm. Its initial density is 0.60 g/cm$^3$ and specific heat 1.26 J/(g K). It is assumed that this value of specific heat applies to the char and ash, as well. At time $t$ = 0, the entire system is at ambient temperature 300 K, the fuel mass fraction $Y_f$ is zero and the oxygen mass fraction is prescribed.

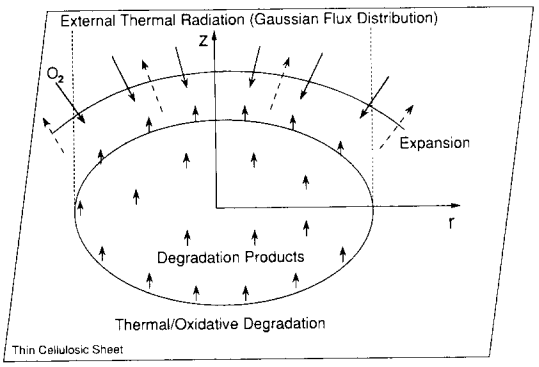


Fig. 1. Schematic of the radiative ignition process.

[3] During the calculation, the heat flux is scaled by the factor $\rho_s/\rho_{s_0}$ to account for the degradation of the sample. There was no noticeable effect on the ignition or flame spread when this scaling of the external radiation was applied. Its implementation was mainly to ensure numerical stability near the region of peak external flux.

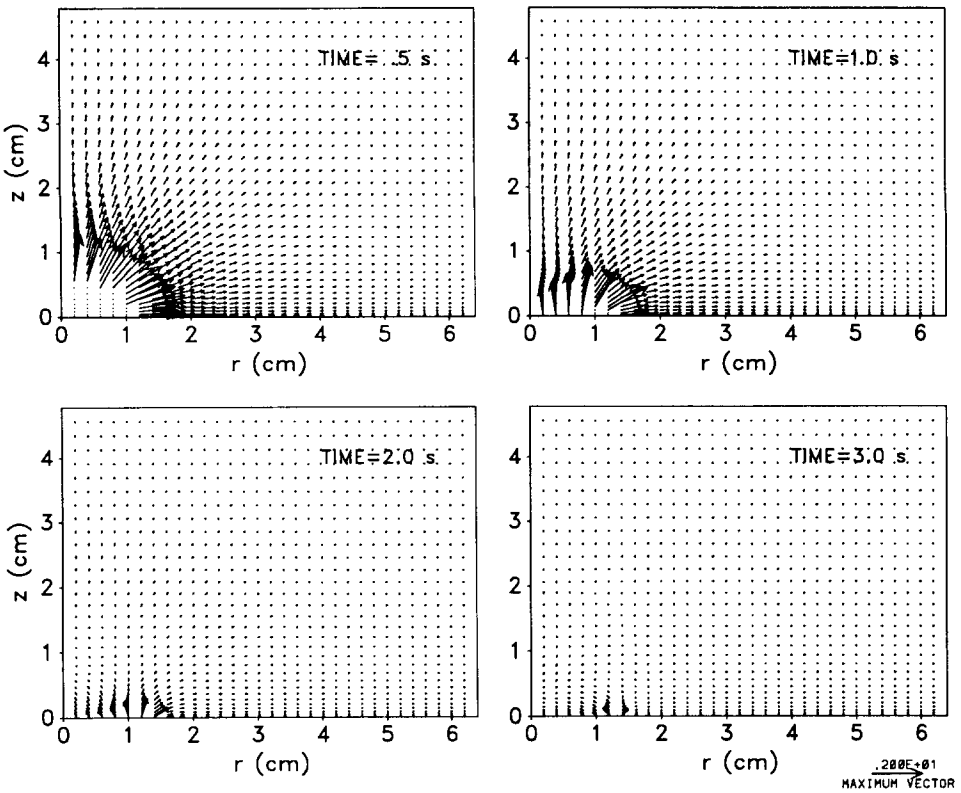


Fig. 2. Velocity vector distribution for 21% oxygen concentration.

The specific heat of the gas $c_p$, density $\rho$, the thermal conductivity $k$, and diffusivity $D$ are considered functions of the temperature $T$, and they are fitted by polynomial expressions. We assume that the gas has the same properties as air. At the reference or ambient temperature 300 K, $c_p = 1.01$ J/(g K), $\rho = 1.19 \times 10^{-3}$ g/cm$^3$, $k = 2.63 \times 10^{-4}$ W/(cm K), and $D = 0.22$ cm$^2$/s. The kinetic constants for the global gas phase oxidation reaction are arbitrarily selected to be: $A = 8.0 \times 10^8$ cm$^3$/(g · s), $E = 6.7 \times 10^4$ J/mol, $\Delta H_f = 3.0 \times 10^4$ J/g, and $\nu = 3.57$. Some studies have been carried out to determine the effect of these constants on the ignition and flame spread.

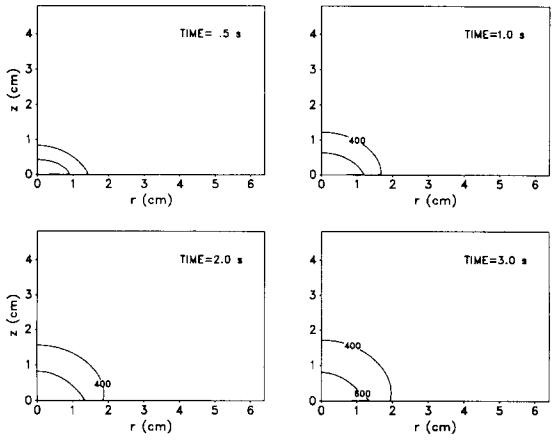


Fig. 3. Gas-phase temperature contours for 21% oxygen concentration. Contours shown start at 400 K and increase in increments of 200.

### 21% Oxygen

The distributions of the flow velocity vectors, temperature, and reaction rate in the gas phase are plotted in Figs. 2–4, respectively. Each figure consists of four plots at different times following the irradiation of the sample. The velocity vector distribution at 0.5 s shows a large amount of evolved gas addition to the gas phase near the center of the sample, which generates a flow velocity approaching 4 cm/s. By 1.0 s, the center part of the sample is nearly converted to char and the evolved gas velocity decreases due to a decrease in the pyrolysis

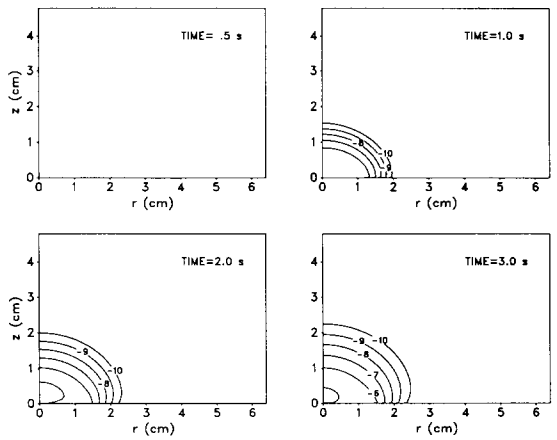


Fig. 4. Gas-phase oxidation reaction rate contours for 21% oxygen concentration. Shown are contours of the quantity $\log_{10} \dot{m}_f$ starting at $-10$ and increasing in increments of 1.

reaction rate. As shown in Fig. 4, the gas-phase reaction is relatively weak near the surface, and the sudden gas expansion and rapid heat release which characterizes ignition does not occur. Note that since the contours are based on the logarithm (base 10) of the reaction rate $\dot{m}_f$, each contour represents a 10-fold change in this quantity.

### 30% Oxygen

For the case of 30% oxygen, ignition occurs at about 1.2 s accompanied by a strong outward expansion due to a large heat release, and the maximum outward flow velocity reaches about 8 cm/s. Figures 5–7 display the flow velocity vectors, temperature and gas-phase reaction rate for this case. The expansion is stronger than that in 21% oxygen and the highest gas temperature approaches 1770 K. The flame at the onset of ignition is umbrella-shaped due to the expansion of the heated gases. The expansion quickly dies down, and by 3.0 s a compression-type flow pattern toward the center part of the sample is formed. In this case, the transition from ignition to flame spread does not occur. The hot gas zone and weak gas-phase

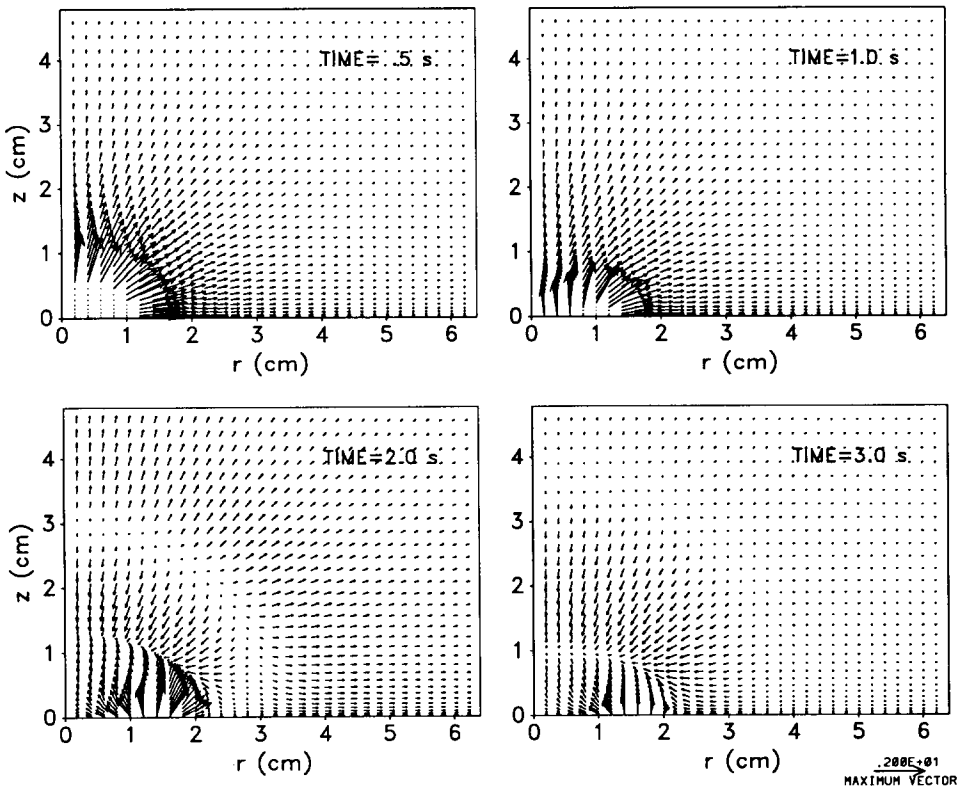


Fig. 5. Velocity vector distribution for 30% oxygen concentration.

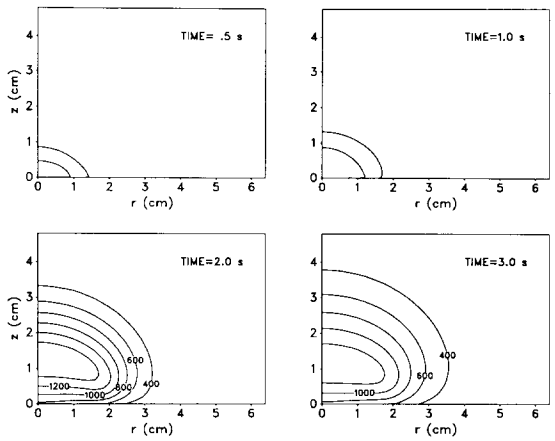


Fig. 6. Gas-phase temperature contours for 30% oxygen concentration. Contours shown start at 400 K and increase in increments of 200.

reaction zone extend radially a little beyond $r = 3$ cm but the active pyrolysis zone shown in Fig. 8 extends only about $r = 2$ cm. The radial distribution of solid surface temperature shown in Fig. 8 indicates a small plateau near 700 K due to the participation of the endothermic pyrolysis reaction after the pre-heating of the sample by the external radiation. Its highest temperature reaches about 750 K at the center. The solid surface sample is heated near $r = 3.5$ cm at 3.0 s, which is well beyond the area irradiated by the external radiation. Since the calculation does not include heat conduction along the radial direction in the sample, the above heating of the sample beyond $r = 2$ cm is only due to heat feedback from the warm gas which flows radially outward from the irradiated area due to the expansion. The heat feedback will be described later in the discussion section. The change in solid density along the radial direction shown in Fig. 8 indicates that after 1.5 s the sample is completely converted to char out to about $r = 1.0$ cm. There is little evidence of char consumption by the char oxidation reaction near the center of the sample in the time scale of this calculation.

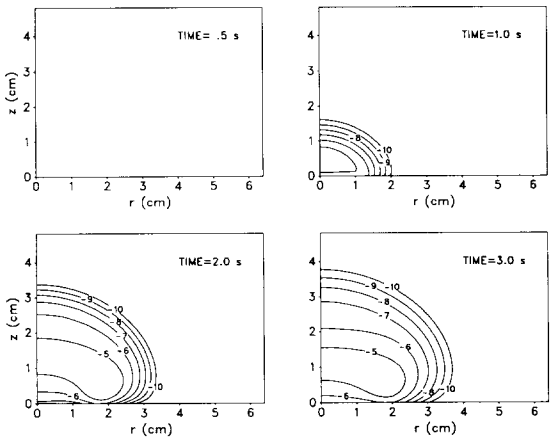


Fig. 7. Gas-phase oxidation reaction rate contours for 30% oxygen concentration. Shown are contours of the quantity $\log_{10} \dot{m}_f$ starting at $-10$ and increasing in increments of 1.

## 50% Oxygen

The calculation was extended to 50% oxygen to look for the possible transition from ignition to flame spread. The calculated distributions of the flow velocity vector, temperature and reaction rate in the gas phase are plotted in Figs. 9–11, respectively. Ignition occurs earlier than in 30% oxygen, and furthermore the transition from ignition to flame spread now occurs. A large outward expansion flow caused by ignition is clearly seen at 1.0 s in Fig. 9. The highest gas temperature is close to 2400 K at the center during the rapid outward expansion

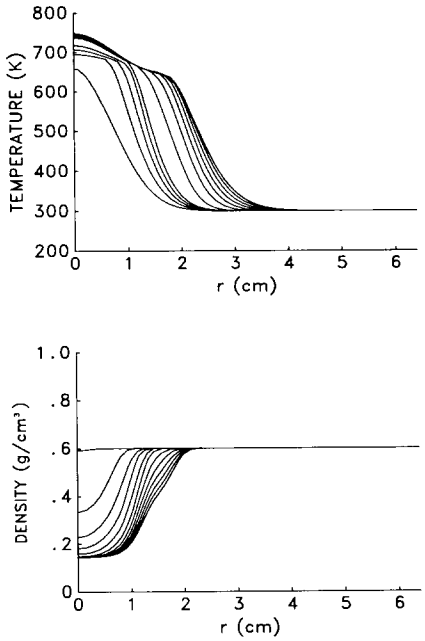


Fig. 8. Radial distribution of sample temperature and density at intervals of 0.25 s for 30% oxygen concentration.

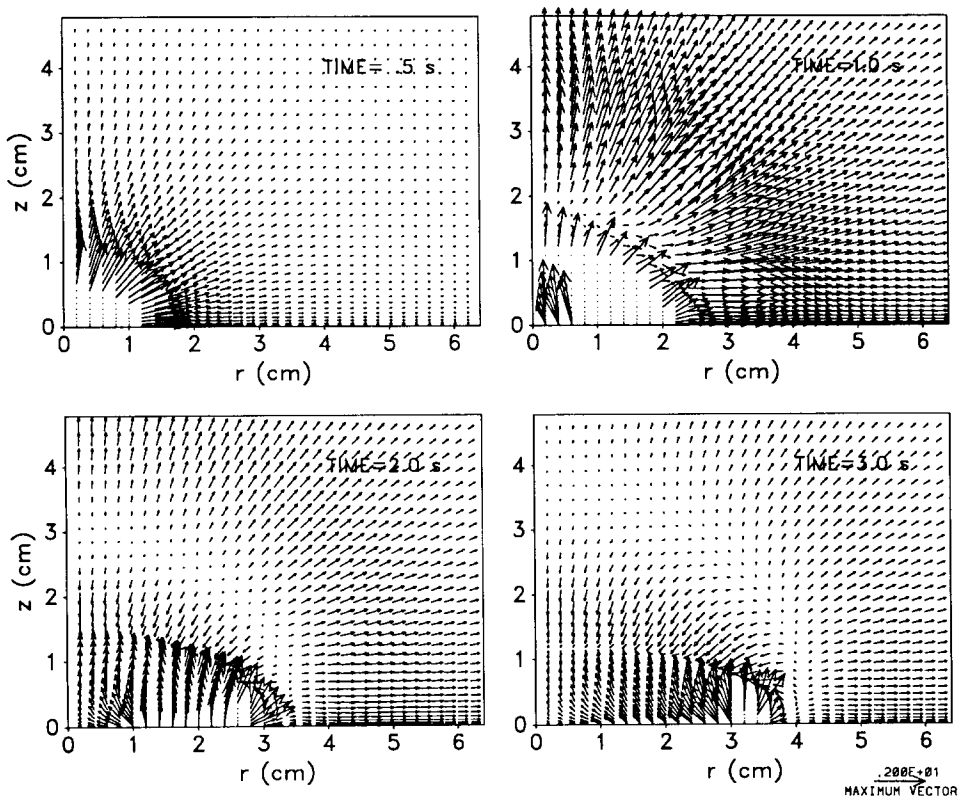


Fig. 9. Velocity vector distribution for 50% oxygen concentration.

following ignition, but the highest temperature in the spreading flame region is about 1750 K. At 2.0 s, the expansion flow becomes weaker, particularly in the axial direction near the center, but by this time the flame is propagating steadily outward. The highest gas phase reaction rate occurs near the sample surface close to $r = 2.7$ cm. If the flame is defined here such that the gas phase reaction rate exceeds $10^{-4}$ g/(cm$^3$ · s), the flame resembles an umbrella

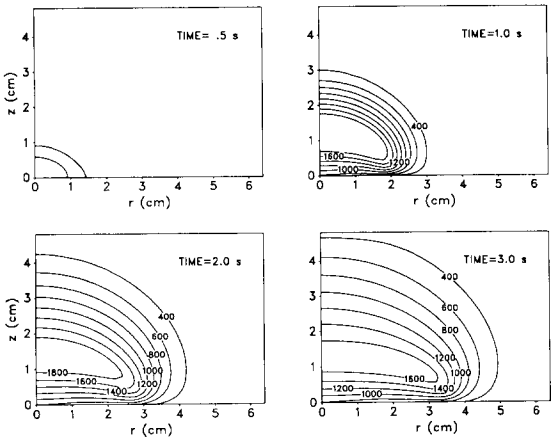


Fig. 10. Gas-phase temperature contours for 50% oxygen concentration. Contours shown start at 400 K and increase in increments of 200.

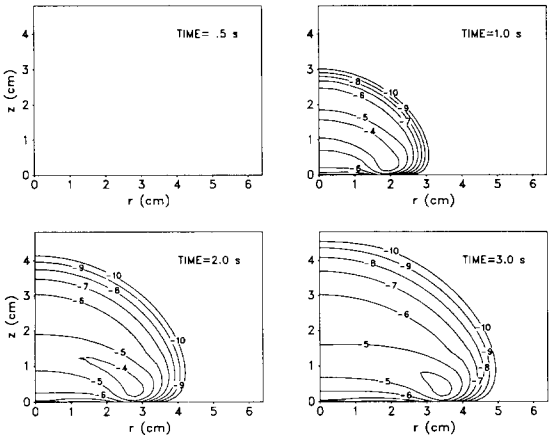


Fig. 11. Gas-phase oxidation reaction rate contours for 50% oxygen concentration. Shown are contours of the quantity $\log_{10} \dot{m}_f$ starting at $-10$ and increasing in increments of 1.

roughly 4 cm in diameter at 1.0 s and 6 cm with a hole in the center at 1.5 s. At 3.0 s, the flame becomes ring-shaped and continues propagating outwards. Since the flame front is very close to the sample surface, it is expected to provide a large amount of energy feedback to the sample in this case, contrary to what was observed in either 21% or 30% oxygen. This case clearly indicates that the transition from ignition to flame spread is attained and the steady outward flame spread rate is about 0.90 cm/s.

Time histories of the sample temperature and density are plotted in Fig. 12. The temperature plateau near 700 K is clearly seen in this figure and the center temperature is slightly higher than that in 30% oxygen due to higher heat feedback from the flame. Using the same definition of flame as discussed above, the location of the traveling flame front at 3.0 s (approximately $r = 3.5$ cm in Fig. 11) is at nearly the same radial location as the pyrolysis front (the first deflection location of the sample density in Fig. 12). The hotter gas extends radially outward much further than the flame front as shown in Fig. 10 and an increase in sample temperature can be seen roughly 1.5 cm ahead of the flame front. Again, there is little evidence of char consumption by the char oxidation reaction in the time considered here.

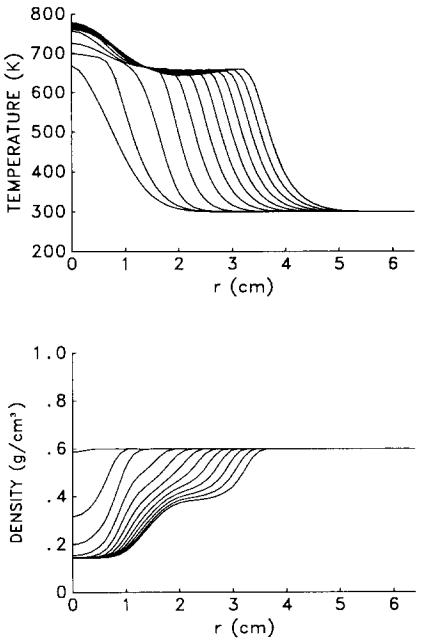


Fig. 12. Radial distribution of sample temperature and density at intervals of 0.25 s for 50% oxygen concentration.

## DISCUSSION

The transition from ignition to flame spread described above occurred only in the case of 50% oxygen. Previous experiments in microgravity [13] showed that the flame spread limit is about 21% oxygen for a single thickness of a different type of paper (Kimwipes, 0.0076 cm thick, density 0.263 g/cm$^3$) and about 26% oxygen for double thickness. The computations with the chosen parameters presented here appear to underpredict the condition for the transition compared with the experimental work. However, there are significant differences between the experiment and these calculations. The experiment was conducted in a two-dimensional configuration with piloted ignition using an electrically powered nichrome wire instead of the axisymmetric configuration and autoignition mode of this calculation. In the autoignition mode, combustible degradation products tend to accumulate more in the gas phase near the heated surface before ignition. This causes a larger expansion of the flow at the onset of ignition and blows the flame further away from the sample surface than does the piloted ignition case. Therefore, the autoignition tends to make the transition from ignition to flame spread more difficult than the piloted ignition. Furthermore, Kimwipe paper was used in the experiment instead of black paper, whose degradation kinetic constants are used for the calculations here.[4]

Since there are significant geometric and material differences between the experiment and the calculation, a few limited attempts

[4] A few calculations were performed in which the density of the sample matched that of the Kimwipes (0.263 g/cm$^3$). The results of the calculations were qualitatively similar to those above (where the sample density was 0.60 g/cm$^3$), although the flame spread rate for the 50% case was about 1.5 cm/s as opposed to 0.9 cm/s found above for the higher density sample. The experiments of Olson for a two-dimensional configuration predict a flame spread rate of 3.8 cm/s for the 50% case.

have been made to adjust the kinetic constants of the gas-phase reaction to obtain a match with the experimental data. For example, it was found that increasing the heat of reaction $\Delta H_f$ from 30,000 to 40,000 J/g increased the flame spread rate by roughly a factor of 3 for the 50% oxygen case. This exercise points out the difficulty in drawing quantitative conclusions from the calculations given the uncertainty of the kinetic constants.

Another exercise was to consider a few calculations with the two-dimensional (line source) configuration using the same chemical and thermal properties and external radiation characteristics as those used for the axisymmetric calculation. The comparison of the results between the two different configurations shows that the onset of ignition and the transition from ignition to flame spread in the two-dimensional configuration tend to be slightly earlier, but the flame spread rates are about the same. In 50% oxygen, the ignition delay is about 25%. It is planned in the future to modify the model to simulate piloted ignition in the two-dimensional configuration.

One of the keys to enabling the transition from ignition to flame spread is the energy feedback rate from the flame to the sample surface. In order to quantify the energy feedback rate and the thermal balance on the thin sample, critical energy fluxes to and losses from the sample are calculated. The results corresponding to the three oxygen concentrations are plotted in Figs. 13–15. $Q_{ex}$ is the external

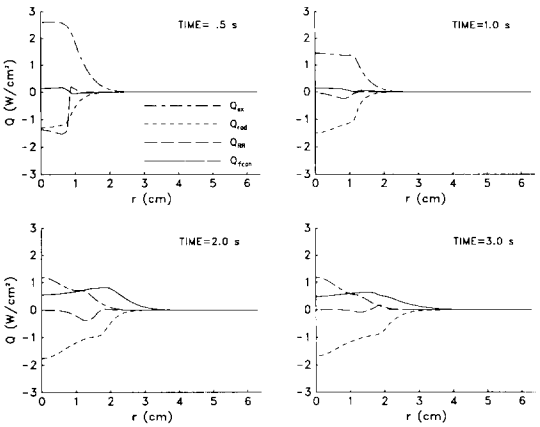


Fig. 14. Energy balance at the surface for 30% oxygen concentration.

thermal radiation, $Q_{rad}$ is re-radiation loss from the sample, $Q_{RR}$ is the net heat (endothermic or exothermic) from the three solid degradation reactions, and $Q_{fcon}$ is the convection/conduction from the gas phase. It is clear from comparing the three plots that this fourth quantity is the key to determining whether or not flame spread will occur. For the 21% case, the convection/diffusion feedback is virtually nonexistent; it is weak in the 30% case, and clearly dominant in the 50% case. Also of interest in these figures is the profile of the net heat from the solid phase reactions $Q_{RR}$. The radial distribution of the amount of endothermic or exothermic heat release rate of each solid-phase reaction in 50% oxygen is shown in Fig. 16. At 0.5 s, a significant heat release from

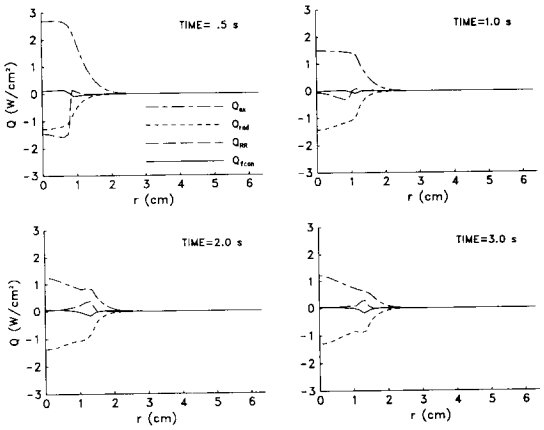


Fig. 13. Energy balance at the surface for 21% oxygen concentration.

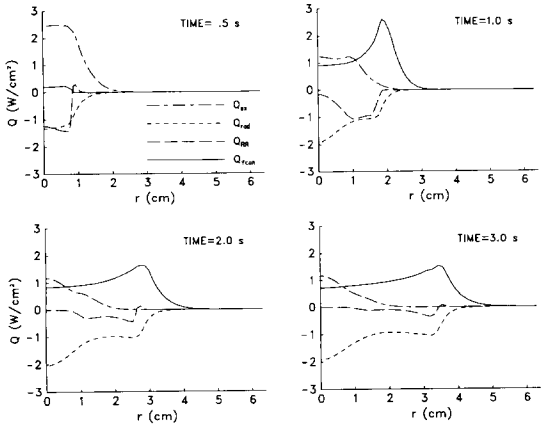


Fig. 15. Energy balance at the surface for 50% oxygen concentration.

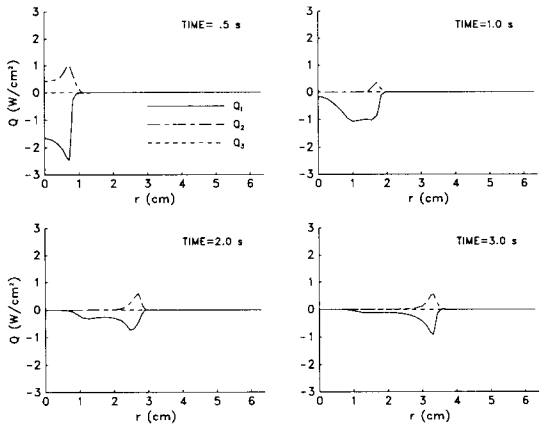


Fig. 16. Contributions of the three solid phase reactions to the quantity $Q_{RR}$.

the exothermic oxidative degradation and a large endothermic pyrolysis reaction can be seen in time and overall the net heat is endothermic. Both reactions become weaker with an increase in time except near the flame front where the net heat release is always endothermic. The exothermic reaction is supported by available oxygen beneath the flame front as shown in Fig. 17. However, there is little contribution of the exothermic char oxidation because oxygen cannot reach the hot char surface in the center part of the sample. The effect of the exothermic oxidative degradation reaction on ignition and flame spread was determined by comparing the results shown in Figs. 10–12 to calculations performed without the exothermic oxidative reaction. The comparison indicates that the inclusion of the exothermic reaction tends to shorten the ignition delay time roughly 15% and increase the flame spread rate about 20% in 50% oxygen.

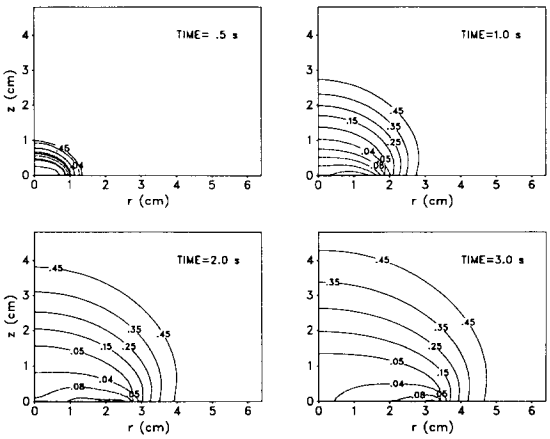


Fig. 17. Fuel (dashed line) and oxygen (solid line) concentrations for the 50% oxygen case at time $T = 3$ s.

In a quiescent microgravity environment, the supply of oxygen has the most significant effect on smoldering [12] and on the transition from ignition to flame spread. Therefore, a flow along the sample surface at even a slow velocity should have significant effects on both processes. The importance of a forced flow on steady flame spread rate has been experimentally demonstrated [13]. Such a study to determine the effects of a slow forced flow on ignition and the transition to flame spread is being undertaken as an extension of the present work. The model is no longer two-dimensional; it becomes three-dimensional. The results will be published in the near future.

## CONCLUSIONS

Autoignition and the subsequent transition from localized ignition to flame spread over a thermally thin cellulosic sheet in a quiescent microgravity environment have been modeled in an axisymmetric configuration and in a two-dimensional configuration and calculated numerically. The results are summarized here.

1. A higher gas-phase oxygen concentration increases the temperature due to an increase in gas-phase reaction rate (and lesser dilution by nitrogen) and thus increases the energy feedback rate to the sample, which increases the supply rate of combustible gaseous degradation products. The transition from ignition to flame spread is controlled by the energy feedback rate.
2. Shortly after ignition, the flame has an umbrella-like shape. The center portion of the flame becomes weaker with time and eventually disappears. Then, a ring-shape flame travels radially outward. The flame near the traveling front is a premixed flame followed by a diffusion flame at its tail.
3. The contribution of the exothermic oxidative degradation reaction to ignition and flame spread is roughly 20% in 50% oxygen

with the chemical and physical values used in this study.

4. The two-dimensional (line source) configuration favors earlier ignition than the axisymmetric configuration. The difference between the two configurations is roughly 25% in 50% oxygen at an external flux of 5 $W/cm^2$ and with the chemical and physical values used in this study. It is also expected that the transition from localized ignition to flame spread is slightly easier in the two-dimensional configuration than in the axisymmetric configuration.

*This study is supported by the NASA Microgravity Science Program under the Inter-Agency Agreement No. C-32000-R. The technical monitor of this study is Dr. Robert Friedman at Lewis Research Center.*

## REFERENCES

1. Kashiwagi, T., *Fire Safety J.* 3:185–200 (1981).
2. Kashiwagi, T., *Combust. Flame* 34:231–244 (1979).
3. Mutoh, N., Hirano, T., and Akita, K., *Seventeenth Symposium (International) on Combustion*, The Combustion Institute, Pittsburgh, 1978, pp. 1183–1190.
4. Akita, K., in *Aspects of Degradation and Stabilization of Polymers* (H. H. G. Jellinek, Ed.), Elsevier, Amsterdam, 1978, Chap. 10.
5. Schiller, D. N., and Sirignano, W. A., 29th Aerospace Sciences Meeting, American Institute of Aeronautics and Astronautics, 1991, Paper AIAA-91-0717.
6. Kashiwagi, T., *Combust. Sci. Technol.* 8:225–236 (1974).
7. Kindelan, M., and Williams, F., *Combust. Sci. Technol.* 16:47–58 (1977).
8. Krishnamurthy, L., *Acta Astronaut.* 3:935 (1976).
9. Amos, B., and Fernandez-Pello, A. C., *Combust. Sci. Technol.* 62:331–343 (1988).
10. Friedman, R., and Sacksteder, K. R., NASA TM100944, December 1988.
11. Smith, R., and Kashiwagi, T., *J. Appl. Fire Sci.* 1-2:103–113 (1990-91).
12. Kushida, G., Baum, H. R., and Kashiwagi, T., *J. Heat Transf.* 114:484–502 (1992).
13. Olson, S. L., Ferkul, P. V., and Tien, J. S., *Twenty-Second Symposium (International) on Combustion*, The Combustion Institute, Pittsburgh, 1988, pp. 1213–1222.
14. Van Dyke, M., *Perturbation Methods in Fluid Mechanics*, Academic, New York, 1964, pp. 149–158.
15. Carrier, G. F., Fendell, F. E., and Marble, F. E., *SIAM J. Appl. Math.* 28:463–500 (1975).
16. Kashiwagi, T., and Nambu, H., *Combust. Flame* 88:345–368 (1992).
17. Wichman, I. S., *Combust. Flame* 83:228–239 (1991).
18. Ito, A., and Kashiwagi, T., *Combust. Flame* 71:189–204 (1988).

*Received 7 June 1993; revised 25 March 1994*